Biochimica et Biophysica Acta 1850 (2015) 1233–1244

Contents lists available at ScienceDirect

Biochimica et Biophysica Acta

journal homepage: www.elsevier.com/locate/bbagen

New enzymatic pathways for the reduction of reactive oxygen species in *Entamoeba histolytica*

Matías S. Cabeza, Sergio A. Guerrero, Alberto A. Iglesias, Diego G. Arias *

Instituto de Agrobiotecnología del Litoral-Facultad de Bioquímica y Ciencias Biológicas (CONICET-Universidad Nacional del Litoral), Santa Fe, Argentina

ARTICLE INFO

Article history:
Received 15 November 2014
Received in revised form 13 February 2015
Accepted 17 February 2015
Available online 25 February 2015

Keywords:
Entamoeba
Rubredoxin
Antioxidant
Flavodiiron-protein
Ferredoxin
Rubrerythrin

ABSTRACT

Background: Entamoeba histolytica, an intestinal parasite that is the causative agent of amoebiasis, is exposed to elevated amounts of highly toxic reactive oxygen and nitrogen species during tissue invasion. A flavodiiron protein and a rubrerythrin have been characterized in this human pathogen, although their physiological reductants have not been identified.
Methods: The present work deals with biochemical studies performed to reach a better understanding of the kinetic and structural properties of rubredoxin reductase and two ferredoxins from *E. histolytica*.
Results: We complemented the characterization of two different metabolic pathways for O_2 and H_2O_2 detoxification in *E. histolytica*. We characterized a novel amoebic protein with rubredoxin reductase activity that is able to catalyze the NAD(P)H-dependent reduction of heterologous rubredoxins, amoebic rubrerythrin and flavodiiron protein but not ferredoxins. In addition, the protein exhibited an NAD(P)H oxidase activity, which generates hydrogen peroxide from molecular oxygen. We describe how different ferredoxins were also efficient reducing substrates for both flavodiiron protein and rubrerythrin.
Conclusions: The enzymatic systems herein characterized could contribute to the in vivo detoxification of O_2 and H_2O_2, playing a key role for the parasite defense against reactive oxidant species.
General significance: To the best of our knowledge this is the first characterization of a eukaryotic rubredoxin reductase, including a novel kinetic study on ferredoxin-dependent reduction of flavodiiron and rubrerythrin proteins.

1. Introduction

Amoebiasis is an intestinal infection widespread throughout the world caused by the human pathogen *Entamoeba histolytica* [CDC, http://www.cdc.gov/]. The parasitic disease is the third leading cause of death in almost all countries where sewage and water quality are inadequate. It causes 50 million clinical episodes of dysentery or amoebic liver abscess and ca. 100,000 deaths annually [WHO, http://www.who.int/en/]. Identification and functional characterization of molecular components are relevant matters not only for the rational design of new therapeutic drugs, but also for the overall knowledge of the parasite biology. In this regard, processes involved in redox metabolism are of particular interest in *E. histolytica* [1,2]. This pathogen has a simple life cycle that comprises an infectious cyst form and an amoeboid trophozoite stage.

E. histolytica trophozoites usually reside and multiply within the human colon, which constitutes a microaerophilic environment [3]. The energy metabolism of this pathogen is exclusively fermentative, with phosphorylation taking place only at the substrate level [4,5]; which shows a strong resemblance to that found in anaerobic bacteria from the genus *Clostridium* [6]. Despite previous studies indicating that *E. histolytica* not only "respires" but also that it has a high affinity for oxygen [7], in aerobiosis the metabolism remains purely fermentative and the transfer of electrons to molecular oxygen is unlikely used for energetic purposes [4,5,8]. In *Giardia lamblia*, another microaerophilic human gastrointestinal eukaryotic parasite, much of the oxygen consumption is due to the activity of a NADH oxidase that catalyzes, without intermediate electron carriers, a four-electron reduction of O_2 to water [9]. The exact physiological function of this enzyme is not clear, and it has been postulated that it could serve to oxidize part of the reduced cofactors produced during fermentative metabolism, thus promoting glycolysis. Also, it has been suggested that the oxygen consumption would serve to protect O_2-labile enzymes such as

Abbreviations: CAT, catalase; CDNB, 1-chloro-2,4-dinitrobenzene; CySNO, *S*-nitrosocysteine; DPI-Cl, diphenyliodonium chloride; DTNB, 5-5′-dithio-nitrobenzoic acid; Fd, ferredoxin; FDP, flavodiiron protein; GOD, glucose oxidase; MAHMA NONOate, 6-(2-hydroxy-1-methyl-2-nitrosohydrazino)-N-methyl-1-hexanamine; MB, methylene blue; MBQ, 2-methyl-benzoquinone; MV, methyl viologen; NROR, NAD(P)H-dependent rubredoxin reductase; Rd, rubredoxin; Rr, rubrerythrin; SOD, superoxide dismutase.

* Corresponding author at: Laboratorio de Enzimología Molecular & Bioquímica Microbiana, Instituto de Agrobiotecnología del Litoral, Centro Científico Tecnológico Santa Fe, Colectora Ruta Nac. N° 168 km. 0, Paraje el Pozo s/n. CP. 3000, Santa Fe, Argentina. Tel./fax: +54 0342 4511370x5023.
E-mail address: darias@fbcb.unl.edu.ar (D.G. Arias).

http://dx.doi.org/10.1016/j.bbagen.2015.02.010
0304-4165/

pyruvate:ferredoxin oxidoreductase (PFOR) [9]. *E. histolytica* has several enzymes with NADH oxidase activity that produce H_2O_2 instead of H_2O as a product [10,11], but the peroxide does not accumulate in viable trophozoites [4,5,8]. So it is unlikely that these enzymes are the functional counterpart of *Giardia* NADH oxidase and therefore probably fulfill another function in vivo.

During tissue invasion, *E. histolytica* is exposed to increased oxygen pressure and high levels of oxidizing reactive oxygen species (ROS) and reactive nitrogen species [RNS, e.g. nitric oxide (NO)] [12,13]. Eukaryotic organisms have various enzyme mechanisms to protect themselves from the deleterious effects of these reactive species [14–17]. *E. histolytica* lacks most of the typical components of the eukaryotic oxidative stress defense systems including catalase, peroxidase, glutathione, and glutathione-recycling enzymes [1,12,18], but has a functional thioredoxin (Trx) system, a 2-Cys peroxiredoxin (2CysPrx), a Fe-superoxide dismutase (FeSOD), two NADPH-oxidoreductases (NO1 and NO2), a rubrerythrin (Rr) and a flavodiiron protein (FDP1) [10,11,19–24]. The non-heme iron-proteins Rr (a peroxidase like protein) and FDP1 (which catalyzes the reduction of O_2 to H_2O) have been characterized as mitosome and cytoplasm residents, respectively. Their enzymatic activities were characterized in vitro as Rd-dependent proteins [19,20]. So far, no Rd encoding-genes were identified in the genome project of *E. histolytica* [1,20], thus no physiological reducing substrate has been described for Rr and FDP1 or metabolic pathway in which they participate. Herein, we analyze the properties of a protein with rubredoxin reductase activity from *E. histolytica* (*Ehi*NROR). The capacity of *Ehi*NROR and amoebic ferredoxins to be physiological substrates to reduce *Ehi*Rr and *Ehi*FDP1 was characterized. Results are analyzed in terms of functionality of metabolic pathways to reduce *Ehi*FDP1 and *Ehi*Rr in the parasite.

2. Materials and methods

2.1. Materials

Bacteriological media components were from Britania Laboratories (Argentina). All other reagents and chemicals were of the highest quality commercially available.

2.2. Data bases

The following data bases were used: NCBI GenBank Data Base (http://www.ncbi.nlm.nih.gov/genbank/) and AmoebaDB genomics resources, an EupathDB project (http://amoebadb.org/amoeba/).

2.3. Bacteria, plasmids, and protozoa

Escherichia coli top 10 cells (Invitrogen) were utilized in routine plasmid construction. *E. coli* M15 (Qiagen) and *E. coli* BL21 (DE3) (Novagen) were employed in expression experiments. The vector pGEM-T Easy (Promega) was selected for cloning and sequencing purposes. The expression vectors were pRSET-A (Invitrogen), pET28c (Novagen) and pQE9 (QIAGEN). DNA manipulations, *E. coli* cultures and transformations were performed according to standard protocols [25]. Cultures of *E. histolytica* (strain HM1-IMSS) were performed under axenic conditions in Diamond's TYI-S-33 medium at 37 °C, and sub-cultured every 72 h [26].

2.4. Molecular cloning

Genes were amplified from *E. histolytica* genomic DNA by PCR techniques. Oligonucleotide primer pairs utilized for PCR amplification were designed from reported spliced sequences (from AmoebaDB, http://amoebadb.org/amoeba/) as described in the Supplementary data — Table 1. Each PCR reaction was performed using *Taq* DNA polymerase (Invitrogen) and the following conditions: 94 °C for 10 min; 30 cycles of 94 °C for 1 min, 45–55 °C for 1 min, and 72 °C for 1 min; then 72 °C for 10 min. The PCR product was subsequently purified and ligated into the pGEM-T easy vector (Promega) to facilitate further works. The sequence of each gene was confirmed on both strands by sequencing.

Constructions obtained into the pGEM-T easy system and the expression vectors were digested with the respective restriction enzymes (Supplementary data — Table 1). The restricted fragments were purified and ligated to the expression vectors using T4 DNA ligase (Promega) during 16 h at 4 °C. Competent *E. coli* BL21 (DE3) cells (Novagen) were transformed with the respective construction by $CaCl_2$ methods. Transformed cells were selected in agar plates containing Luria–Bertani broth (LB, 10 g/l NaCl; 5 g/l yeast extract; 10 g/l peptone; pH 7.4) supplemented with ampicillin (100 μg/ml) and/or kanamycin (50 μg/mL).

2.5. Expression and purification

Single colonies of *E. coli* BL21 (DE3) transformed with each of the recombinant plasmid were picked to inoculate TB broth (24 g/l yeast extract; 12 g/l peptone; 5 g/l glycerol; 17 mM KH_2PO_4; 72 mM K_2HPO_4; pH 7.4) supplemented with 23 μg/ml ferric ammonium citrate, 100 μg/ml ampicillin and/or 50 μg/ml kanamycin, and grown overnight at 37 °C with shaking at 180 rpm. The overnight culture was diluted (1/100) in fresh media and grown under identical conditions to exponential phase, OD_{600} of ~0.6. The expression of the respective recombinant protein was induced with 0.5 mM IPTG, followed by incubation at 25 °C. After 16 h the cells were harvested and stored at −20 °C until use. The bacterial pellet was suspended in binding buffer (20 mM Tris–HCl pH 7.5, 10 mM imidazole and 400 mM NaCl) and disrupted by sonication. The lysate was centrifuged (16000 ×*g*, 30 min) to remove cell debris. Purification of each recombinant protein was performed under aerobic conditions using a HiTrap IMAC-Ni^{2+} column (1 ml, GE). The HiTrap IMAC-Ni^{2+} column was loaded with the prepared extract and washed with 15 volumes of binding buffer. The recombinant protein was eluted with elution buffer (20 mM Tris–HCl pH 7.5, 300 mM imidazole and 400 mM NaCl). Active fractions were pooled and stored at −80 °C with 20% (v/v) glycerol. Under the specified storage conditions, the recombinant proteins remained fully active for one year after their purification.

Thioredoxins from *E. histolytica* (*Ehi*Trx8 and *Ehi*Trx41), rubredoxin reductase from *Thermotoga maritima* (*Tma*NROR), rubredoxin from *Pyrococcus furiosus* (*Pfu*Rd) and rubredoxin from *Clostridium pasteurianum* (*Cpa*Rd) were expressed in *E. coli* BL21 (DE3) as His-tagged (N-term) recombinant proteins, and they were chromatographically purified as previously described [23,24,27–29]. Purified ferredoxin NADP reductase from *Pisum sativum* (*Psa*FNR), ferredoxin from *P. sativum* (*Psa*Fd) and flavodoxin from *E. coli* (*Eco*Fld) were kindly provided by Dr. E.A. Ceccarelli (IBR — Rosario, Argentina).

2.6. Protein methods

Protein concentration was determined by the method of Bradford [30], utilizing BSA as standard. SDS-PAGE was carried out using the Bio-Rad minigel equipment, basically according to previously described methods [31].

Sera anti-*Ehi*NROR and anti-*Ehi*FDP1 were prepared by rabbit immunization, while anti-*Ehi*Rr prepared by mice immunization. In all cases, the purified recombinant proteins were used as an immunogen according to Vaitukaitis et al. [32]. Amoebic protein extracts were prepared suspending the parasite pellets in lysis buffer (50 mM Tris–HCl, pH 7.5, 1% SDS). Proteins in SDS-PAGE gel were blotted onto a nitrocellulose membrane. The membrane was blocked overnight at 4 °C with 5% skimmed milk in PBS, subsequently incubated with primary antibody at room temperature for 1 h, and then incubated with a HRP-conjugated anti-rabbit secondary antibody for 1 h. Bands were visualized using the ECL Western blotting detections reagents (Thermo Scientific).

2.7. Determination of the apparent molecular mass by gel filtration chromatography

Native molecular mass of proteins was determined by gel filtration chromatography in a Superdex 200 HR Tricorn column (GE). The calibration curve was constructed plotting the logarithm of the molecular mass (log Mr) vs the distribution coefficients (K_{av}) measured for each protein standard: thyroglobulin (669 kDa), ferritin (440 kDa), aldolase (158 kDa), conalbumin (75 kDa), ovalbumin (43 kDa), carbonic anhydrase (29 kDa), ribonuclease A (13.7 kDa) and aprotinin (6.5 kDa) (Gel Filtration Calibration Kit — GE).

2.8. Preparation of CySNO

CySNO was prepared as previously described [33] by nitrosation under acid conditions. Briefly, equal volumes of cysteine (200 mM) and sodium nitrite (200 mM) were incubated in the presence of 10 mM HCl on ice for 30 min. Freshly prepared CySNO was stabilized by the addition of 1 mM EDTA at pH 7.0 and stored on ice in the dark until use. The concentration of CySNO was estimated by measuring absorbance at 332 nm, using a molar absorption coefficient of 0.75 mM^{-1} cm^{-1} [33].

2.9. Flavin and iron determination

Purified *Ehi*NROR or *Ehi*FDP1 was boiled in the dark for 10 min and centrifuged to remove the denatured protein. The cofactor in the respective protein was visualized after resolving the supernatant (at room temperature and in the dark) by thin layer chromatography (TLC) on silica sheets 25 TLC ALUMINIUM plates (Merck). The mobile phase was a solution of butanol:acetic acid:water (12:3:5). The chromatogram was analyzed by fluorescence with the *Typhoon* scanner (GE Healthcare). A solution of commercial FAD or FMN was used as a standard. After identification of the flavin, its concentration was quantified spectrophotometrically using the molar extinction coefficient at 450 nm of 11.3 mM^{-1} cm^{-1} [34].

Iron quantification was performed using the ferric thiocyanate method [10]. Briefly, a sample protein (25 μl) plus TCA 40% (5 μl) was incubated at 4 °C for 10 min. Then, the mix was centrifuged at 16000 ×*g* and 4 °C for 15 min and the supernatant was recovered. In a final reaction volume of 100 μl, 10 μl of supernatant was mixed (in this order) with 80 μl of TCA 4% and 10 μl of 2.5 M KSCN. The absorbance of the generated red color was measured at 492 nm. The iron concentration was calculated utilizing $FeCl_3$ as the standard.

2.10. Enzymatic assays and kinetic analysis

All enzymatic assays were performed spectrophotometrically at 30 °C using a Multiskan Ascent one-channel vertical light path filter photometer (Thermo Electron Co.). In all the cases the final volume was of 50 μl (with a light path of 0.5 cm), in degassed (unless otherwise stated) 100 mM potassium phosphate buffer pH 7.0.

Rubredoxin reductase activity of *Ehi*NROR was measured in microaerophilic conditions by monitoring Rd reduction at 492 nm with 2 mM Glc, 10 U/ml GOD, 20 U/ml catalase (CAT), 10 U/ml superoxide dismutase (SOD), 0.3 mM NAD(P)H, 0.1–100 μM *Pfu*Rd or *Cpa*Rd, and 0.005–0.1 μM *Ehi*NROR. For steady-state kinetic analysis, assays were performed using 10 nM *Ehi*NROR.

Thioredoxin reductase activity of *Ehi*NROR was measured in microaerophilic conditions by monitoring NADPH oxidation at 340 nm with 2 mM Glc, 10 U/ml GOD, 20 U/ml CAT, 10 U/ml SOD, 0.3 mM NAD(P)H, 0.13 mM bovine insulin, 0.15–30 μM *Ehi*Trxs, and 0.1–1 μM *Ehi*NROR.

Activity for 5,5′-dithiobis(2-nitrobenzoic acid) (DTNB) reductase of *Ehi*NROR was measured by monitoring the production of thionitrobenzoate at 405 nm (ε = 14.5 mM^{-1} cm^{-1} [35]) with 2 mM Glc, 10 U/ml glucose oxidase (GOD), 20 U/ml CAT, 10 U/ml SOD, 0.3 mM NADPH, 0.078–10 mM DTNB, and 0.1–1 μM *Ehi*NROR. For steady-state kinetic analysis, assays were performed using 0.1 μM *Ehi*NROR.

The capacity of *Ehi*NROR for cystine or CySNO reduction was measured by monitoring the oxidation of NAD(P)H at 340 nm in the presence of 0.3 mM NAD(P)H, 0.1–1 μM *Ehi*NROR and 15–1000 μM cystine or CySNO. For steady-state kinetic analysis, assays were performed using 0.1 μM *Ehi*NROR.

Diaphorase activity of *Ehi*NROR was measured by monitoring the oxidation of NAD(P)H at 340 nm in the presence of 0.3 mM NAD(P)H, 0.1–1 μM *Ehi*NROR and as final acceptor substrate: 2–500 μM 2-methyl-benzoquinone (MBQ), 15–1000 μM $Fe(CN)_6^{3-}$ or methylene blue (MB). For steady-state kinetic analysis, assays were performed using 50 nM *Ehi*NROR.

NAD(P)H-dependent nitrite or hydroxylamine reductase activity of *Ehi*NROR was measured by monitoring the oxidation of NAD(P)H at 340 nm in the presence of 0.3 mM NAD(P)H, 0.1–1 μM *Ehi*NROR and 15-1000 μM $NaNO_2$ or NH_2OH.

Transhydrogenase activity of *Ehi*NROR was measured by monitoring the reduction of S-NAD^+ at 400 nm (ε = 12 $mM^{-1}\cdot cm^{-1}$ [36]) with 0.3 mM NADPH, 0.1–1 μM *Ehi*NROR and 0.2 mM S-NAD^+.

Free flavin reduction by *Ehi*NROR was measured by monitoring the reduction of FAD or FMN at 450 nm (ε = 11.3 mM^{-1} cm^{-1} [37]) in the presence of 0.3 mM NAD(P)H, 0.1–1 μM *Ehi*NROR and 3–200 μM FAD or FMN.

Nitroreductase activity of *Ehi*NROR was measured by monitoring the oxidation of NADPH at 340 nm with 0.3 mM NADPH, 10–1000 μM *1*-chloro-*2,4*-dinitrobenzene (CDNB) or methyl-viologen (MV), and 0.1–1 μM *Ehi*NROR. For steady-state kinetic analysis, assays were performed using 50 nM *Ehi*NROR.

NAD(P)H oxidase activity of *Ehi*NROR was determined by the oxidation of NAD(P)H at 340 nm in oxygenated 100 mM potassium phosphate buffer plus 0.1–1 μM *Ehi*NROR. Hydrogen peroxide and superoxide anion (O_2^-) production due to NAD(P)H oxidase activity of the enzyme were determined with the ferrithiocyanate method [38] and by monitoring the reduction of nitro blue tetrazolium (NBT) by O_2^- [39], respectively. For steady-state kinetic analysis, assays were performed using 0.1 μM *Ehi*NROR.

The NADPH-dependent O_2-reduction by *Ehi*NROR was performed at pH 7.0 and 30 °C under anaerobic conditions (in N_2-saturated reaction mixtures) with 0.3 mM NADPH, 0.1 μM *Ehi*NROR and different concentrations of O_2. Molecular oxygen pulses were generated enzymatically by CAT and different concentrations of H_2O_2. The O_2 reduction was followed by monitoring of NADPH oxidation at 340 nm.

Rubrerythrin reduction was evaluated by the measurement of peroxidase activity of *Ehi*Rr using different redox proteins as donor substrates. Assays were performed monitoring the NAD(P)H oxidation at 340 nm with 2 mM Glc, 10 U/ml GOD, 10 U/ml SOD, 0.1–10 μM *Ehi*Rr, 25 μM H_2O_2 and different donor substrates (and their enzymatic system): 1) 0.3 mM NADPH, 1 μM *Psa*FNR and 0.1–10 μM *Eco*Fld, *Psa*Fd, *Ehi*Fd1 or *Ehi*Fd2. 2) 0.3 mM NADH, 1 μM *Tma*NROR and 0.1–10 μM *Pfu*Rd. 3) 0.3 mM NAD(P)H and 0.1–1 μM *Ehi*NROR. For steady-state kinetic analysis of *Ehi*Rr-reduction by *Ehi*NROR, assays were performed using 0.1 μM *Ehi*NROR.

Superoxide dismutase activity of *Ehi*Rr was detected monitoring the inhibition of NBT reduction by O_2^- [39,40]. The assays were performed monitoring the reduction of NBT at 540 nm under aerobic conditions with 2 mM Glc, 1 U/ml GOD, 20 U/ml CAT and 5–20 μM *Ehi*Rr. One unit of superoxide dismutase is defined as the amount of protein that caused 50% inhibition of the rate of NBT reduction.

Flavodiiron protein reduction was evaluated by the measurement of the molecular oxygen (O_2) or nitric oxide (NO) reductase activity of *Ehi*FDP1 using different redox proteins as donor substrates in aerobic or microaerophilic conditions, respectively. The assays were performed monitoring the NAD(P)H oxidation at 340 nm in oxygenated (for O_2

reductase activity) or degassed (for NO reductase activity) conditions with 0.05–5 μM *Ehi*FDP1 and different donor substrates (and their enzymatic system): 1) 0.3 mM NADPH, 1 μM *Psa*FNR and 0.1–10 μM *Eco*Fld, *Psa*Fd, *Ehi*Fd1 or *Ehi*Fd2. 2) 0.3 mM NADH, 1 μM *Tma*NROR and 0.1–10 μM *Pfu*Rd. 3) 0.3 mM NAD(P)H and 0.1–1 μM *Ehi*NROR. Under microaerophilic conditions, it was added to reaction media 2 mM Glc, 10 U/ml GOD, 20 U/ml CAT, 10 U/ml SOD and 1 mM MAHMA NONOate (as NO donor for NO reductase activity of *Ehi*FDP1). For steady-state kinetic analysis of *Ehi*FDP1-reduction by *Ehi*NROR, assays were performed using 50 nM *Ehi*NROR.

All kinetic data were plotted as initial velocity ($\mu M \cdot min^{-1}$) versus substrate concentration. The kinetic parameters were acquired by fitting the data with a nonlinear least-squares formula and the Michaelis–Menten equation using the program Origin. Kinetic constants are the mean of at least three independent sets of data, and they were reproducible within ± 10%. IC_{50} refers to the concentration of the inhibitor giving 50% of the initial activity.

2.11. Immunolocalization by confocal microscopy

Trophozoites of *E. histolytica* (strain HM1-IMSS) obtained from axenic cultures were washed twice for 15 min at room temperature in a phosphate buffered saline solution (PBS; 8 g/l NaCl, 0.2 g/l KCl, 1.44 g/l Na_2HPO_4, 0.24 g/l KH_2PO_4, pH 7.4) and fixed in 4% (v/v) formaldehyde. After washing they were permeabilized and blocked during 30 min in a medium containing PBS plus the addition of 0.1% (v/v) Triton X-100 and 3% (w/v) BSA. Fixed samples were incubated first with specific polyclonal antibodies (1/100 dilution) and thereafter with FITC-conjugated goat anti-rabbit antibody and TRITC-conjugated goat anti-mouse antibody (both 1/1000 dilution). Incubation with the primary and secondary antibodies was performed at 25 °C during 1 h. After washing, the slides were finally mounted with antifade mounting solution plus DAPI and visualized under a confocal microscope (DIC/Nomarski, Eclipse TE-2000-E2 — Nikon, Facility).

3. Results

3.1. Identification, molecular cloning and recombinant expression of ehinror, ehifd1, ehifd2, ehiRr and ehifdp1 genes from E. histolytica

Based on the information available in the data base of the *E. histolytica* genome project (http://amoebadb.org/amoeba/), we identified and amplified by PCR the gene coding for a putative rubredoxin reductase (previously identified as NADH oxidase, EHI_153000) from genomic DNA. The amplified sequence was cloned into pGEM-T easy and its identity was confirmed by full sequencing. The gene (1344 bp in length) is predicted to encode a 447-amino-acid protein (*Ehi*NROR) with a molecular mass of 49.7 kDa and a calculated pI of 8.2. Domain analysis with the servers NCBI CD-Search (http://www.ncbi.nlm.nih.gov/), Pfam (http://pfam.sanger.ac.uk/) and Prosite (http://prosite.expasy.org/) revealed that the protein belongs to the FAD-dependent pyridine nucleotide reductases family. This family includes a number of related enzymes such as glutathione reductase, thioredoxin reductase, rubredoxin reductase, ferredoxin:$NADP^+$ reductase, nitrite reductase, glutamate synthase, and NADH oxidase [41]. Analysis of *Ehi*NROR primary sequence allowed us to identify a FAD-binding motif (^{49}EVVIIGGGIASLSVIRCLI^{67}) and a NAD(P)H-binding domain (^{197}QIAIIGAGLSGIEISNALR^{215}) (Supplementary data — Fig. 1). BLAST search revealed homologous proteins distributed among *Clostridium* species with an identity of ~29%. Several of these proteins are putative rubredoxin reductases. The closest bacterial homologue is a putative NADH-dependent rubredoxin reductase from *Clostridium tetani* (NCBI: NP_783044.1).

An amino acid sequence alignment between *Ehi*NROR and rubredoxin reductases already characterized shows a limited sequence identity (lower than 22%) and the presence in the former of an N-terminal extension (Supplementary data — Fig. 1). Two potential pairs of metal chelating Cys are present in the *Ehi*NROR N-terminal extension, being the separation among them shorter (in primary sequence) than for other rubredoxin-like domain (Supplementary data — Fig. 2). This extension is also present in the *C. tetani* homologue which harbors a rubredoxin-like domain. To characterize the functionality of this putative *Ehi*NROR, the protein was expressed in *E. coli* M15 as a protein fused to an N-terminal His-tag, using the pQE-9 vector. *Ehi*NROR was produced in a soluble form and conveniently purified by a single Ni^{2+} affinity chromatography step. The molecular mass revealed for the recombinant protein (~50 kDa) by SDS-PAGE agrees with the size deduced from their respective DNA-derived amino acid sequence (Supplementary data — Fig. 2-A).

Five encoding genes for putative [4Fe–4S] ferredoxins (EHI5A_055540; EHI5A_067050; EHI5A_003410; EHI_099860 and KM1_013210) were also identified in the *E. histolytica* genome project data base. We amplified *ehifd1* (EHI5A_055540, 180 bp) and *ehifd2* (EHI5A_067050, 210 bp) from genomic DNA of *E. histolytica* by PCR and cloned into the pGEM-T Easy vector for analysis. *ehifd1* (180 bp) and *ehifd2* (210 bp) encode two proteins with a theoretical molecular mass of 6.05 kDa (pI of 4.12) and 7.37 kDa (pI of 4.40), respectively. Based on bioinformatic tools, we performed amino acid sequence alignment of these proteins and also a domain prediction analysis (using Prosite servers). The study revealed a high sequence identity between *Ehi*Fds and [4Fe4S] Fds, including the four key Cys residues for iron–sulfur cluster binding (Supplementary data — Fig. 3). Genes encoding *Ehi*Fd1 and *Ehi*Fd2 were cloned into pET28c and expressed in *E. coli* BL21 (DE3) cells as recombinant proteins with a His-tag in their respective N-terms. Soluble fractions were purified chromatographically, to obtain amoebic Fds with purity higher than 98%, as judged by SDS-PAGE (Fig. 1-A). The molecular mass determined for each protein was of ~10 kDa, which agrees with the expected size deduced from their DNA-derived amino acid sequence, plus ~2 kDa of the N-term His-tag.

Rubrerythrin has a rubredoxin-like FeS4 center and a hemerythrin-like binuclear iron cluster and presents H_2O_2-peroxidase activity [19,28,42]. Previously, Maralikova et al. [19] showed that the amino acid sequence of *Ehi*Rr contains all residues involved in chelating iron atoms in highly conserved form and also that the protein exhibits a peroxidase activity (with a heterologous electron donor system). Furthermore, they showed that the enzyme localized in mitosomes. Herein, the gene coding for *Ehi*Rr (EHI_134810) was amplified by PCR from genomic DNA, and its identity was confirmed by DNA sequencing. *Ehi*Rr is a predicted protein with 189 amino acid residues, with a molecular mass of 21.2 kDa and a theoretical pI of 6.36. The protein shares sequence identity with characterized orthologous Rrs from *Desulfovibrio vulgaris* (GI: 238472; 35%) and *P. furiosus* (GI: 18893381; 31%). Pure recombinant protein migrated as a single band of ~25 kDa in reducing SDS-PAGE (Supplementary data — Fig. 2-A), presumably because of additional N-terminal residues that incorporate the His-tag.

Recently Vicente et al. [20] reported the characterization of a flavodiiron protein from *E. histolytica* (*Ehi*FDP1) which is a bacterial-type oxygen/nitric oxide reductase. The authors demonstrated the protein functionality using an in vitro electronic transfer chain consisting of *E. coli* flavorubredoxin oxidoreductase and the isolated rubredoxin domain from *E. coli* flavorubredoxin. To this point, no putative physiological redox partners for *Ehi*FDP1 have been identified in the entamoeba cell. In order to evaluate the capacity of amoebic Fds as possible physiological partners of *Ehi*FDP1, we cloned the gene coding for *Ehi*FDP1 (EHI5A_235560) into the pET28c vector and expressed it in *E. coli*, to produce the recombinant protein. After IMAC, *Ehi*FDP1 migrated as a single band of 49 kDa in reducing SDS-PAGE (Supplementary data — Fig. 2-A).

3.2. Biophysical properties of recombinant EhiNROR, EhiRr and EhiFDP1

Purified *Ehi*NROR showed no difference in its electrophoretic migration when it was analyzed by non-reducing SDS-PAGE (data not

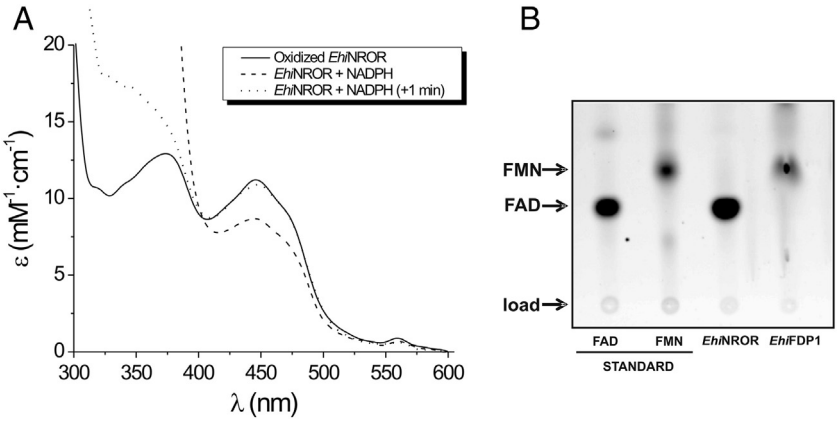

Fig. 1. UV–visible absorption spectrum of *Ehi*NROR and identification of the flavin as FAD by thin layer chromatography. A) UV–vis spectrum of purified *Ehi*NROR at 25 °C and pH 7.0. Solid line: oxidized *Ehi*NROR, dash line: *Ehi*NROR + 50 μM NADPH and dot-line: *Ehi*NROR 1 min after the addition of NADPH. B) Determination of flavin by thin layer chromatography. Chromatography was revealed by fluorescence with the *Typhoon* scanner.

shown). In addition, after native thiol titration with DTNB we determined a [R-SH]/[*Ehi*NROR] ratio of 21.2 ± 0.4. These results reveal that all Cys residues in *Ehi*NROR are in the thiol (R-SH) form (21 Cys residues are present in the primary structure of the enzyme); suggesting that, a priori, no inter- or intra-molecular disulfide bond is present in the enzyme. Moreover, the purified *Ehi*NROR eluted as a ~41 kDa protein in gel filtration chromatography (Supplementary data — Fig. 2-B), suggesting that the enzyme has a monomeric structure in its native state. The latter is in agreement with previous reports on Rd reductase and NADH oxidase proteins from other sources [9,41,43].

The presence of flavin in the purified *Ehi*NROR was verified by UV–visible spectroscopy. The protein exhibited absorption peaks at 450 and 375 nm (Fig. 1-A), which is characteristic for the spectra of these flavoprotein family members [44]. As shown in Fig. 1-A, aerobic addition of NADPH caused a decrease in the absorbance at 450 nm and an increase at 560 nm. As described elsewhere [44,45], the decrease in the absorbance at 450 nm corresponds to the reduction of the flavin prosthetic group in *Ehi*NROR. In most flavoproteins the cofactor is tightly but not covalently bound and this seems to be the case for *Ehi*NROR. Hence, a bright yellow compound was released after protein denaturalization by boiling the purified *Ehi*NROR for 10 min. Analysis by thin-layer chromatography of the resulting prosthetic group showed that *Ehi*NROR contains a FAD cofactor (Fig. 1-B). Furthermore, the flavin content of the recombinant *Ehi*NROR was calculated in approximately 1.2 ± 0.3 mol FAD/mol of protein. Despite its potential N-terminal rubredoxin-like domain, iron could not be detected in the protein even in the case of being produced in a medium supplemented with the metal (data no shown). The latter is consistent with the result of the thiol titration, in which all Cys residues were detected in the free thiol form in the absence of any chelating agent.

The *Ehi*Rr protein eluted as a dimer (M_r ~ 53 kDa) when analyzed by gel filtration chromatography (Supplementary data — Fig. 2-B), in agreement with structures reported for characterized rubrerythrin from prokaryotes [42]. Furthermore, the iron content of the isolated recombinant *Ehi*Rr was calculated to be ~3.4 ± 0.6 mol Fe/mol of protein. This finding indicates a full occupancy of metal ions in the protein. The absorption spectrum of oxidized *Ehi*Rr and the bleaching produced by reduction with sodium dithionite are shown in the Supplementary data — Fig. 4-A. As previously reported, absorption peaks at 494 nm and 580 nm are mainly due to the rubredoxin-like FeS4 center, while that at 370 nm represents combined absorptions from the rubredoxin-like FeS4 center and the hemerythrin-like binuclear iron cluster [42].

The recombinant *Ehi*FDP1 was eluted as a native dimer protein (M_r ~ 100 kDa) when analyzed by gel filtration chromatography (Supplementary data — Fig. 2-B). The iron content of the purified protein was determined in 2.3 ± 0.2 mol Fe/mol of protein (full occupancy). Prosthetic group analysis by thin-layer chromatography indicated that *Ehi*FDP1 contains the cofactor FMN (Fig. 1-B), in a ratio of 1.1 ± 0.1 mol FMN/mol of protein. The absorption spectrum of oxidized and reduced (with dithionite) *Ehi*FDP1 is show in the Supplementary data — Fig. 4-B.

3.3. EhiNROR has NAD(P)H dependent H_2O_2 and O_2^- generating oxidase activity

Under aerobic conditions, *Ehi*NROR showed an NAD(P)H oxidase activity using molecular oxygen as the final acceptor (Fig. 2-A). As experimental control, in the absence of O_2 (by saturating the reaction buffer with N_2) no NAD(P)H oxidase activity was observed (data no shown). In addition, we evaluated the putative production of H_2O_2 by *Ehi*NROR by the measurement of the hydrogen peroxide using the ferric thiocyanate method. *Ehi*NROR produced H_2O_2 by partial reduction of dissolved O_2 in the reaction mixture, with rates comparable to those determined for NADPH or NADH oxidation (Fig. 2-B). We also evaluated the enzyme-dependent O_2^- production using the NBT reduction assay. As shown in Fig. 2-C, when the reaction mixtures containing NADPH and NBT (under aerobic conditions) were supplemented with diverse concentrations of *Ehi*NROR, the rates of NBT reduction were increased proportionally. Furthermore, the aerobic NBT reduction by *Ehi*NROR was stimulated or inhibited by the presence of CAT or SOD, respectively (see Fig. 2-C). These results indicate that *Ehi*NROR generates O_2^- as a sub-product associate to O_2 reduction.

In order to characterize the chemical groups and putative cofactors involved in the oxidase activity of *Ehi*NROR, we evaluated the inhibition profile of different compounds (Fig. 2-D). The NADPH oxidase activity of *Ehi*NROR was significantly sensible to Cu^{2+} (IC_{50} = 0.4 μM), Hg^{2+} (IC_{50} = 1.4 μM) and Zn^{2+} (IC_{50} = 4 μM). No effect was observed with other bivalent cations, such as Ca^{2+}, Mg^{2+}, Mn^{2+}, Co^{2+} or Ni^{2+} (data not shown). Fig. 2-D illustrates about inhibition exerted by iodoacetamide (an alkylating agent) and oxidized coenzymes ($NADP^+$ and NAD^+) on this enzymatic activity. The latter is analyzed in more details below. Neither EDTA nor azide (agents that modify protein metal centers) produced enzyme inhibition. These results support the participation of Cys residues in the active site for NAD(P)H oxidase activity of this enzyme. In addition, diphenyliodonium chloride (a specific flavoprotein inhibitor [46]) acted as a strong inhibitor of NAD(P)H oxidase activity of *Ehi*NROR (Fig. 2-D), regardless of coenzyme evaluated (IC_{50} = 4.4 μM). This result supports the idea that the NAD(P)H oxidase activity is dependent on the presence of FAD in the protein.

The NAD(P)H oxidase activity of *Ehi*NROR exhibited hyperbolic kinetics for NAD(P)H oxidation and O_2 reduction (Fig. 3). Table 1 shows the kinetic parameters for oxygen-dependent oxidation of NAD(P)H

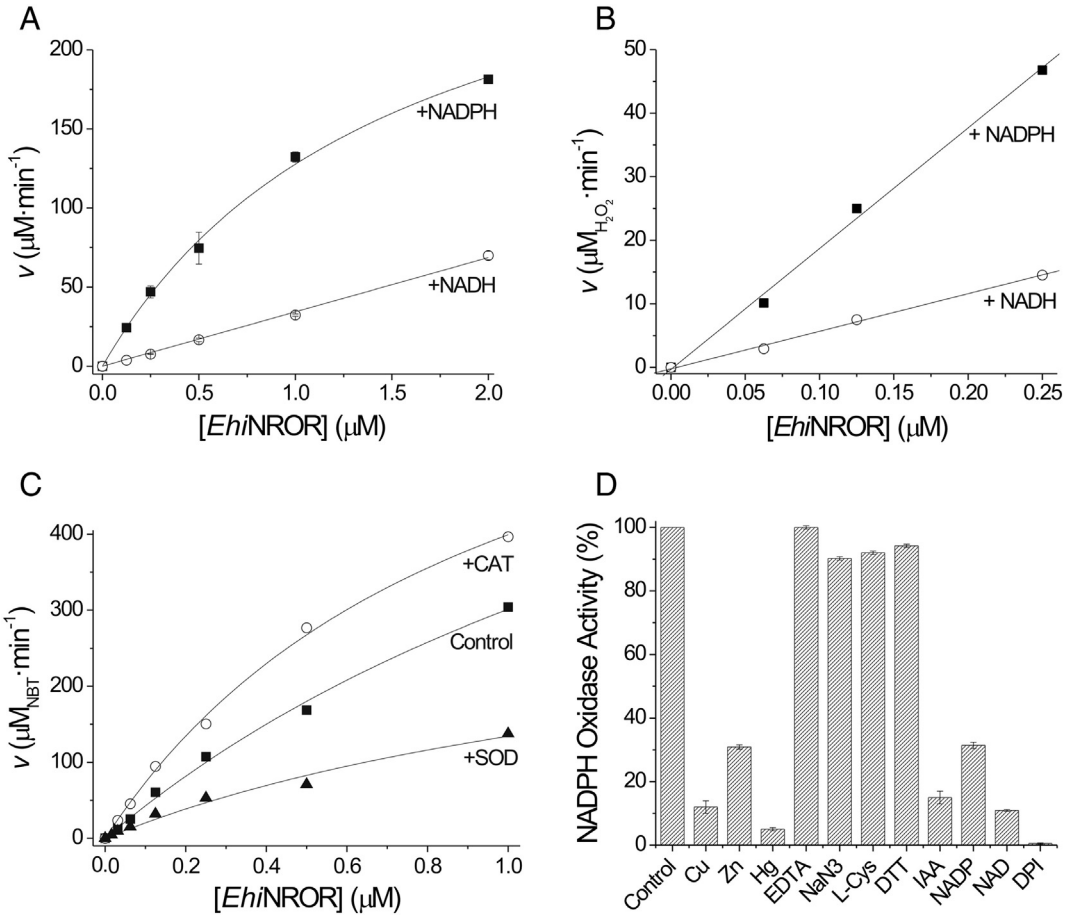

Fig. 2. NAD(P)H oxidase activity of *Ehi*NROR in aerobic conditions. A) NAD(P)H oxidase activity of *Ehi*NROR (at 340 nm). Reactions were performed at pH 7.0 and 30 °C with 300 μM of NADPH (■) or 300 μM of NADH (○) and different concentrations of *Ehi*NROR. B) H_2O_2 production by *Ehi*NROR. Reactions were performed at pH 7.0 and 30 °C in the presence of 300 μM of NADPH (■) or 300 μM of NADH (○) and the specified concentrations of *Ehi*NROR. Generated H_2O_2 was detected using the ferrithiocyanide method. C) NBT-reduction by generated O_2^- by *Ehi*NROR. The reactions were performed at pH 7.0 and 30 °C in the presence of 300 μM of NADPH, different concentrations of *Ehi*NROR in the absence or presence of commercial catalase (CAT) or superoxide dismutase (SOD). D) Effect on NADPH oxidase activity of *Ehi*NROR by different compounds. Reactions were performed at pH 7.0 and 30 °C with 300 μM of NADPH and different compounds: Cu^{2+}, Zn^{2+}, Hg^{2+} and diphenyliodonium chloride (DPI-Cl) at 100 μM; EDTA, sodium azide, L-Cys, DTT, iodoacetic acid (IAA), $NADP^+$ and NAD^+ at 1 mM. Control assay was performed without reagents.

and O_2-reduction by *Ehi*NROR. The enzyme exhibited high affinity for O_2 and the catalytic efficiency exhibited by this enzyme for NADPH is higher than for NADH. The latter is a remarkable difference with respect to other NRORs, exhibiting a high specificity toward NADH [9,29,41].

3.4. Reductase activity of EhiNROR with low molecular mass substrates

We evaluated the capacity of *Ehi*NROR to reduce low molecular mass substrates. The activity was measured by means of NADPH-dependent

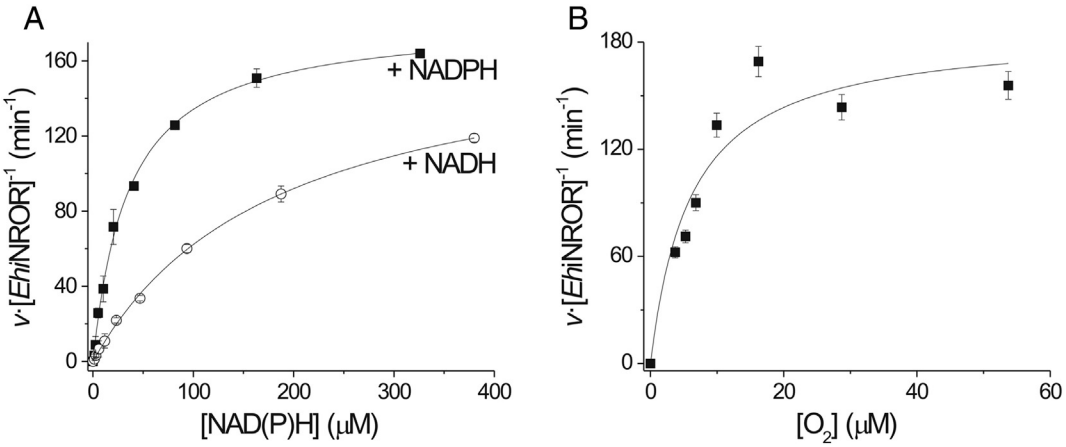

Fig. 3. Oxygen-dependent oxidation of NAD(P)H kinetics. A) NAD(P)H oxidation kinetics by *Ehi*NROR. The kinetic assays were performed at pH 7.0 and 30 °C under aerobic conditions with different concentrations of NADPH (■) or NADH (○) and 0.1 μM *Ehi*NROR. B) NADPH-dependent O_2-reduction by *Ehi*NROR. The kinetic assays were performed at pH 7.0 and 30 °C under anaerobic conditions (in N_2-saturated reaction mixtures) with 0.3 mM NADPH, 0.1 μM *Ehi*NROR and different concentrations of O_2. Molecular oxygen pulses were generated enzymatically by CAT and different concentrations of H_2O_2. The O_2 reduction was followed by monitoring of NADPH oxidation at 340 nm.

Table 1
Apparent kinetic parameters of *Ehi*NROR at pH 7.0 and 30 °C.

Cosubstrate	Substrate	*K*m (μM)	k_{cat} (min^{-1})	$k_{cat}\cdot Km^{-1}$ ($M^{-1}\cdot s^{-1}$)
O_2 ~ 200 μM	NADPH	36 ± 3	182 ± 5	$8.4 \cdot 10^4$
	NADH	183 ± 15	176 ± 9	$1.6 \cdot 10^4$
NADPH	CySNO	243 ± 22	116 ± 4	$8.0 \cdot 10^3$
300 μM	DTNB	468 ± 32	8.7 ± 0.2	$3.1 \cdot 10^2$
	$Fe(CN)_6^{3-}$	183 ± 28	2879 ± 320	$2.6 \cdot 10^5$
	MV	162 ± 22	64 ± 3	$6.5 \cdot 10^3$
	CDNB	110 ± 11	1080 ± 36	$1.6 \cdot 10^5$
	*Pfu*Rd	3.2 ± 0.2	574 ± 13	$3.0 \cdot 10^6$
	*Cpa*Rd	2.8 ± 0.5	832 ± 63	$5.0 \cdot 10^6$
	*Ehi*Rr[a] (*Ehi*NROR)	0.45 ± 0.03	264 ± 23	$9.8 \cdot 10^6$
	*Ehi*Rr[a] (*Ehi*NRORΔ47N)	0.46 ± 0.04	99 ± 2	$3.6 \cdot 10^6$
	*Ehi*FDP1[b] (*Ehi*NROR)	0.39 ± 0.03	51 ± 1	$2.2 \cdot 10^6$
	*Ehi*FDP1[b] (*Ehi*NRORΔ47N)	0.44 ± 0.03	28 ± 2	$1.1 \cdot 10^6$
	O_2	6 ± 2	187 ± 21	$5.2 \cdot 10^5$
NADH	$Fe(CN)_6^{3-}$	40 ± 6	6298 ± 243	$2.6 \cdot 10^6$
300 μM	CDNB	105 ± 15	87 ± 6	$1.4 \cdot 10^4$
	*Pfu*Rd	5.2 ± 0.7	4166 ± 274	$1.3 \cdot 10^7$
	*Cpa*Rd	4.3 ± 0.6	2158 ± 129	$8.4 \cdot 10^6$
	*Ehi*Rr[a]	0.50 ± 0.02	262 ± 21	$8.7 \cdot 10^6$
	*Ehi*FDP1[b]	0.40 ± 0.06	42 ± 2	$1.7 \cdot 10^6$

[a] Peroxidase activity with 25 μM H_2O_2.
[b] NO reductase activity with 1 mM MAHMA NONOate.

reduction of H_2O_2, methylene blue (MB), $Fe(CN)_6^{3-}$, methyl viologen (MV), 1-chloro-2,4-dinitrobenzene (CDNB), NO_2^-, FAD, FMN, NH_2OH or 2-methy-benzoquinone (MBQ) following an absorbance decrease at 340 nm or an increase at 450 nm for FAD/FMN reduction. The kinetic data indicated that only $Fe(CN)_6^{3-}$, MV and CDNB acted as electron acceptor substrates for the enzyme and their reduction followed the Michaelis–Menten kinetics (Table 1). These results suggest that the enzyme has activities of NAD(P)H-dependent ferric-reductase and nitroreductase exhibiting an enzymatic behavior and kinetic parameters similar to those previously reported for other NRORs [28,43,47]. For NADPH-dependent ferric-reductase activity of *Ehi*NROR, enzyme inhibition was detected at high $Fe(CN)_6^{3-}$ concentrations (higher than 300 μM), which followed a substrate inhibition kinetic (K_{is} = 393 ± 80 μM at 30 °C and pH 7.0 (Supplementary data — Fig. 5), whereas no enzyme inhibition was observed when NADH was used as a reducing substrate (Supplementary data — Fig. 5). On the other hand, reduction of CDNB by *Ehi*NROR was more efficient with NADPH than with NADH (Supplementary data — Fig. 6).

Different low molecular mass disulfides were evaluated as possible acceptor substrates of *Ehi*NROR. In our hands, no activity was detected with lipoamide, glutathione disulfide or cystine as substrates (up to 1 mM, data not shown). A slight disulfide reductase activity was observed with DTNB as a substrate, which reduction followed the Michaelis–Menten kinetics (Table 1) with low catalytic efficiency. On the other hand, we investigated the capacity of *Ehi*NROR to reduce *S*-nitrosothiols, such as CySNO. Under microaerophilic conditions, *Ehi*NROR exhibited NADPH-dependent reduction of CySNO following the Michaelis–Menten kinetics (Table 1). Catalytic efficiency value for CySNO reduction is comparable with that reported for the *E. histolytica* thioredoxin reductase [10].

3.5. EhiNROR presents a non-specific rubredoxin reductase activity

The enzyme showed activity as NAD(P)H-dependent rubredoxin reductase (Fig. 4), using bacterial Rd (from *C. pasteurianum* and *P. furiosus*) as final substrates. This activity exhibited a maximum at pH 7.0 (at 30 °C — data not shown). The catalytic efficiency for Rd reduction using NADH is higher than for NADPH (in equivalent concentration). An analysis of the obtained kinetic parameters indicated that the difference in the catalytic efficiency is due to changes in the k_{cat} rather than the *K*m values for the reduction of Rd (Table 1).

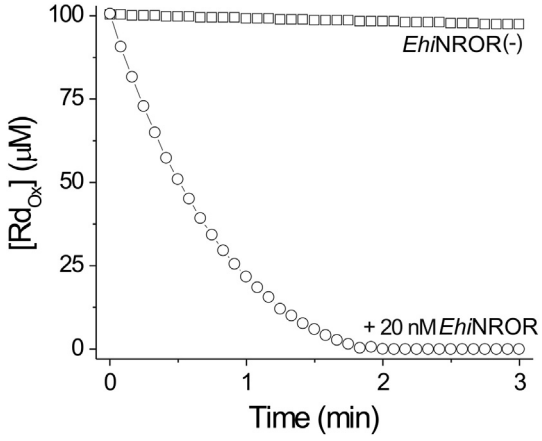

Fig. 4. NADH-dependent reduction of *Cpa*Rd by *Ehi*NROR. Assays were performed at 30 °C and pH 7.0 in microaerophilic conditions by monitoring Rd reduction at 492 nm. The reaction mixture contained 200 μM NADH, 100 μM *Cpa*Rd and absence (□) or presence (○) of 20 nM *Ehi*NROR.

Additionally, no substrate inhibition was observed at high NAD(P)H (up to 300 μM, data no shown). Results in Table 1 indicate that *Ehi*NROR exhibited high affinity values toward heterologous Rds (Table 1) and high catalytic efficiencies for Rd reduction (Table 1), being similar to those parameters determined for NRORs from other species [43,47].

Genes for rubredoxin are absent in the genome of *E. histolytica* [1,20], so the putative physiological substrate of *Ehi*NROR is unknown. We first considered that the enzyme could be transferring reduction equivalents from NAD(P)H to Fd or Trx, which are abundant in this parasite [11,24,48,49]. No reductase activity was detected when Rd was replaced with *Ehi*Fd1, *Ehi*Fd2 or *Psa*Fd (for ferredoxin reductase activity); *Eco*Fld (flavodoxin reductase activity); and *Ehi*Trx8 or *Ehi*Trx41 (for Trx reductase activity). These results encouraged us to in-depth investigate the physiological role of *Ehi*NROR and its cellular substrates. It presents an Rd-like redox active domain [19,42], as discussed below.

3.6. EhiRr and EhiFDP1-reductions are efficiently mediated by amoebic Fds

As a first approach, we observed that the purified recombinant *Ehi*Rr showed a redoxin-dependent peroxidase activity. The activity was determined by coupled NAD(P)H-dependent assays, using H_2O_2 as a peroxide substrate in combination with Rd (from *P. furiosus*), Fld (from *E. coli*) or [2Fe2S]Fd (from *P. sativum*) as reduction substrates. The apparent k_{cat} values calculated for these substrates (at pH 7.0 and 30 °C) were 100.3 min^{-1}, 17.5 min^{-1} and 26.3 min^{-1}, respectively. No peroxidase activity was detected when amoebic Trxs were used as a redox donor for *Ehi*Rr (data not shown). These results suggest that not only Rd can be used as a reducing substrate, as described in bacteria [28]. Other redoxin proteins that have a different type of redox center, such as iron–sulfur cluster (Fd) or flavin (Fld or other flavoprotein) exhibited redox activity with EhiR. In view of these results, we evaluated the ability of amoebic Fds (*Ehi*Fd1 and *Ehi*Fd2) to transfer reducing equivalents to *Ehi*Rr, following NADPH oxidation in the presence of FNR from *P. sativum* (for Fd regeneration). The amoebic Fds were able to transfer reduction equivalents to *Ehi*Rr with an enzymatic efficiency similar than *Pfu*Rd (in the presence of *Tma*NROR for Rd regeneration). The reduction of *Ehi*Rr by amoebic Fd or Rd followed hyperbolic kinetics, with parameters detailed in Table 2.

We further characterized *Ehi*Rr evaluating its ability to reduce H_2O_2 using *Pfu*Rd and *Ehi*Fds as substrates. *Ehi*Rr showed a high catalytic efficiency for H_2O_2 reduction (Table 2) independently of the reducer utilized (Supplementary data — Fig. 7-A). This catalytic efficiency might indicate that in vivo *Ehi*Rr would be an efficient mitosomal peroxidase. In addition, this value is similar to that calculated for amoebic peroxiredoxin [24]. High H_2O_2 concentrations (higher than 25 μM)

Table 2
Apparent kinetic parameters of *Ehi*Rr and *Ehi*FDP1 at pH 7.0 and 30 °C.

Protein	Cosubstrate	Substrate	Km (μM)	k_{cat} (min^{-1})	$k_{cat}\cdot Km^{-1}$ ($M^{-1}\cdot s^{-1}$)
*Ehi*Rr	H_2O_2 25 μM	*Ehi*Fd1	2.7 ± 0.4	432 ± 26	$2.7 \cdot 10^6$
		*Ehi*Fd2	1.3 ± 0.2	465 ± 30	$6.0 \cdot 10^6$
		*Pfu*Rd	3.7 ± 0.5	620 ± 40	$2.8 \cdot 10^6$
	*Ehi*Fd1 10 μM	H_2O_2	>25 μM	N.D.	$2.2 \cdot 10^5$
	*Ehi*Fd2 10 μM		>25 μM	N.D.	$2.0 \cdot 10^5$
	*Pfu*Rd 10 μM		>25 μM	N.D.	$3.3 \cdot 10^5$
*Ehi*FDP1	O_2 ~ 200 μM	*Ehi*Fd1	2.3 ± 0.2	716 ± 30	$5.2 \cdot 10^6$
		*Ehi*Fd2	3.0 ± 0.3	852 ± 42	$4.7 \cdot 10^6$
		*Pfu*Rd	>10 μM	N.D.	$8.0 \cdot 10^4$
	*Ehi*Fd1 10 μM	NO[a]	102 ± 12	17.2 ± 0.6	$2.8 \cdot 10^3$
	NO-reductase activity: $k_{cat\ app} = 15.5 \pm 0.3\ min^{-1}$ (with 10 μM *Ehi*Fd1 and 1 mM MAHMA NONOate)				
	O_2-reductase activity: $k_{cat\ app} = 337 \pm 10\ min^{-1}$ (with 10 μM *Ehi*Fd1 and ~200 μM O_2)				

[a] Generated with MAHMA NONOate.

inhibited the catalytic activity of *Ehi*Rr with a $K_{is} = 167 \pm 26$ μM at 30 °C and pH 7.0 (Supplementary data — Fig. 7-A). The obtained data showed a linear behavior up to 25 μM H_2O_2 ($R^2 = 0.95$). Due to this linear behavior, it was not possible to fit the data to a Michaelis–Menten model and thus determine a *K*m value. In view of the linear increase of the reaction rate with the concentration of H_2O_2 up to 25 μM, it is possible to assume that the *K*m must be greater than this value. In addition, we determined that *Ehi*Rr has a superoxide dismutase (SOD) activity when assayed with the standard method of inhibition of NBT reduction. Oxidized *Ehi*Rr exhibited SOD activity, being able to inhibit the reduction of NBT by dismutation of superoxide with a specific activity of 96 $U\cdot mg^{-1}$ at pH 7.0 and 30 °C (Supplementary data — Fig. 7-B), a value similar to that previously reported for Rr from *Clostridium perfringens* [50]. In addition, a slight superoxide reductase activity (in the presence of CAT) was detected when Rd from *P. furiosus* was used as an electron donor (apparent $k_{cat} = 1.8 \pm 0.1\ min^{-1}$ at pH 7.0 and 30 °C).

As mentioned previously, no putative physiological redox partner for *Ehi*FDP1 has been identified in the entamoebic cell. In order to evaluate the capacity of amoebic Fds (*Ehi*Fd1 and *Ehi*Fd2) to transfer reducing equivalents to *Ehi*FDP1 (as possible physiological partners), we evaluated the oxygen reductase activity (under aerobic conditions) of *Ehi*FDP1 using an NAD(P)H-dependent coupled assay in the presence of FNR from *P. sativum* (for Fd regeneration). Fig. 5 shows that amoebic

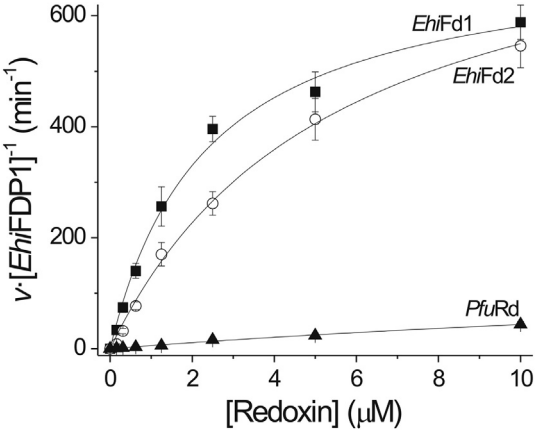

Fig. 5. Reduction of *Ehi*FDP1 by amoebic Fds and *Pfu*Rd. *Ehi*FDP1 reduction was evaluated by the measurement of O_2 reductase activity of *Ehi*FDP1 using different redox proteins as donor substrates under aerobic conditions. The assays were performed monitoring the NAD(P)H oxidation at 340 nm in oxygenated 100 mM potassium phosphate buffer, pH 7.0 and 30 °C with 0.05 μM *Ehi*FDP1 and different donor substrates (and their enzymatic system): 0.3 mM NADPH, 1 μM *Psa*FNR and 0.1–10 μM *Ehi*Fd1 (■); 0.3 mM NADPH, 1 μM *Psa*FNR and 0.1–10 μM *Ehi*Fd2 (□) or 0.3 mM NADH, 1 μM *Tma*NROR and 0.1 — 10 μM *Pfu*Rd (▲).

Fds were able to transfer reduction equivalents to *Ehi*FDP1 more efficiently than *Pfu*Rd (in the presence of *Tma*NROR for Rd regeneration). The reduction of *Ehi*FDP1 for amoebic Fds followed hyperbolic kinetics. In contrast, the reduction of the protein by *Pfu*Rd exhibited no saturation kinetic (Fig. 5). Table 2 reports the kinetic parameters calculated of *Ehi*FDP1 reduction. Interestingly, we observed than [2Fe2S]Fd from *P. sativum* and both amoebic Fds exhibited similar reduction capacity (data no shown).

3.7. EhiNROR is an alternative reductant for EhiRr and EhiFDP1 under microaerophilic conditions

To evaluate the transfer of electrons from *Ehi*NROR to *Ehi*Rr, we measured the peroxidase activity of *Ehi*Rr using *Ehi*NROR as the reducing substrate. On the other hand, to evaluate the reduction of *Ehi*FDP1 by *Ehi*NROR, we measured the nitric oxide reductase activity of *Ehi*FDP1 [20] (because *Ehi*NROR presents an intrinsic oxygen reductase activity that interferes with the determination of the same activity in *Ehi*FDP1) using MAHMA NONOate as an NO donor in the reaction medium. Under microaerophilic conditions, in the absence of redoxins as a mediator, *Ehi*Rr or *Ehi*FDP1 reduction by *Ehi*NROR followed Michaelis–Menten kinetics with similar catalytic efficiencies (Table 1). Conversely, under aerobic conditions, no activity of *Ehi*NROR was detected for *Ehi*Rr or *Ehi*FDP1 reduction (data not shown). The reduction of both *Ehi*Rr and *Ehi*FDP1 by *Ehi*NROR did not show differences in their kinetic parameters when NADPH or NADH was used as reduction equivalent sources (Table 1). In addition, no activity was evident when one of the components was omitted in the reaction media.

As mentioned above, *Ehi*NROR presents an N-terminal extension that resembles an Rd-like domain. This domain retains the four putative chelating Cys, although the separation between them is shorter than expected. Moreover, an extra Cys is present in the N-terminal extension of *Ehi*NROR. Interestingly, no iron was detected with the ferrithiocyanate method in the recombinant *Ehi*NROR, which was further supported by the fact that the incubation of *Ehi*NROR with an excess of EDTA (molar ratio protein:EDTA of 1:100) did not affect its ability to transfer reducing equivalents to *Ehi*Rr (data no shown). To understand the role of the N-terminal extension in the electron transfer cascade, we decided to construct a truncated version of *Ehi*NROR (*Ehi*NRORΔ47N) in which the first 47 amino acids were eliminated. The NADPH oxidase activity of *Ehi*NRORΔ47N (130 ± 5 min^{-1} at pH 7.0 and 30 °C) was not affected, with respect to that measured for *Ehi*NROR (120 ± 3 min^{-1} at pH 7.0 and 30 °C), however, the truncated protein exhibited an impaired ability to transfer electrons to *Ehi*FDP1 (Fig. 6-A) or *Ehi*Rr (Fig. 6-B). The calculated k_{cat} parameter was 2-fold lower for the truncated enzyme, remaining the *K*m values without modifications in both cases (Table 1). For *Ehi*Rr reduction (Fig. 6-C), a complementation between *Ehi*NRORΔ47N and *Pfu*Rd (in 1:1 ratio) let them to reach an activity value equivalent to that obtained with *Ehi*NROR (in the absence of *Pfu*Rd). Thus, despite the N-terminus is not directly involved in the electron transfer due to the absence of iron (or other metal ion) as a cofactor, it appears to fulfill a role in protein interactions.

3.8. NADPH oxidase but not ferric-reductase activity of EhiNROR is strongly inhibited by NAD^+

We evaluated the inhibitory capacity of $NADP^+$ or NAD^+ on the NAD(P)H oxidase activity (under aerobic conditions) exhibited by *Ehi*NROR by means of titration at a fixed concentration of NAD(P)H (2.5-fold *K*m). The titration profile indicated that $NADP^+$ acted as a poor inhibitor with respect to NADH, with an $IC_{50} \gg 1000$ μM, whereas in NAD^+, the IC_{50} was 1050 μM. On the other hand, $NADP^+$ showed a mild effect inhibitor with respect to NADPH (IC_{50} of 430 μM) being NAD^+ a notably better inhibitor with respect to NADPH (IC_{50} of 0.5 μM). As experimental control, using S-NAD^+ (instead of NAD^+ in order to detect its reduction at 405 nm) we found that the inhibitory

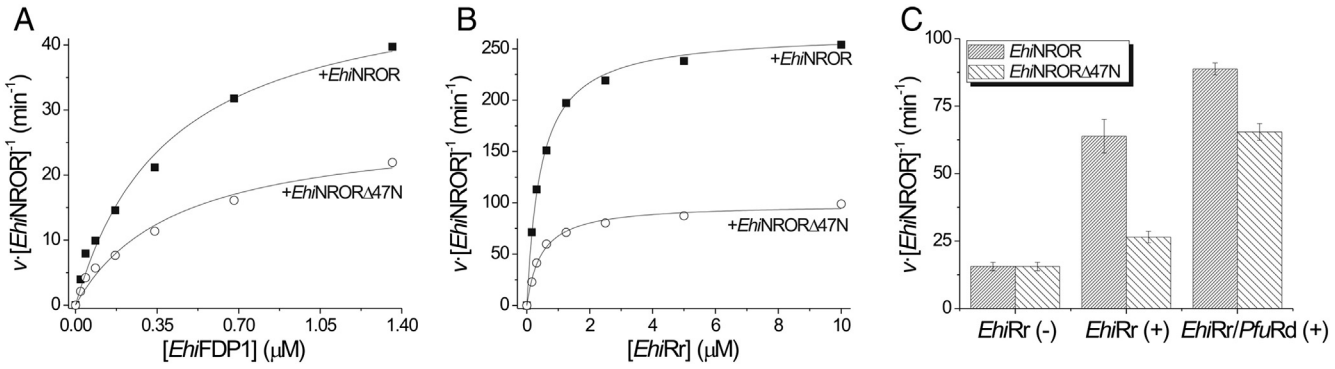

Fig. 6. Direct *Ehi*FDP1 or *Ehi*Rr reduction by *Ehi*NROR. A) Kinetics of *Ehi*FDP1-reduction by *Ehi*NROR assayed under anaerobic conditions at pH 7.0 and 30 °C in the presence of 0.3 mM NADPH, 1 mM MAHMA NONOate, different concentrations of *Ehi*FDP1 (0.02 to 1.4 μM) and 0.05 μM *Ehi*NROR (■) or *Ehi*NRORΔ47N (○). B) Kinetics of *Ehi*Rr-reduction by *Ehi*NROR assayed under anaerobic conditions at pH 7.0 and 30 °C in the presence of 0.3 mM NADPH, 25 μM H_2O_2, different concentrations of *Ehi*Rr (0.1 to 10 μM) and 0.1 μM *Ehi*NROR (■) or *Ehi*NRORΔ47N (○). C) In vitro complementation of *Ehi*NRORΔ47N with *Pfu*Rd. Assays were performed under anaerobic conditions at pH 7.0 and 30 °C in the presence of 0.3 mM NADPH, 25 μM H_2O_2, 5 μM *Ehi*Rr, 0.1 μM *Ehi*NROR or *Ehi*NRORΔ47N, in the absence or in the presence of *Pfu*Rd (0.1 μM).

behavior was not an artifact due to a possible transhydrogenase activity of *Ehi*NROR, which was not detected. We re-evaluated the effect of NAD^+ on the NADPH oxidase activity exhibited by *Ehi*NROR at different NADPH concentrations. As shown in the Supplementary data — Fig. 8, inhibition profiles were similar and, apparently, NADPH concentration-independent (resembling noncompetitive inhibition). These assays yielded an average IC_{50} of 0.23 ± 0.03 μM, a value very close to the enzyme concentration used in the assay (~0.1 μM). This would indicate that for NADPH oxidase activity, NAD^+ could act as a tight-binding inhibitor (interacting very strongly with *Ehi*NROR). However, ferric-reductase activity of *Ehi*NROR (with ferricyanide, *Pfu*Rd or *Ehi*Rr) was not significantly inhibited by NAD^+ (IC_{50} > 50 μM, Fig. 7).

3.9. EhiNROR is expressed in trophozoites and co-localizes with EhiRr in mitosome

The occurrence of *Ehi*NROR in *E. histolytica* was confirmed by western blotting utilizing specific polyclonal antibodies, as shown in the Supplementary data — Fig. 9. The antibodies were also useful to study the subcellular localization of the protein by confocal immunofluorescence, with results illustrated by Fig. 8. Despite the fact that the amino acid sequence of *Ehi*NROR lacks predictable signal peptide regions, the microscopy images revealed recognition signals distributed in the whole parasite cell with a punctuated fluorescence patterns, co-localizing with *Ehi*Rr (a mitosomal protein [19], Fig. 8). This would indicate that *Ehi*NROR has mitosomal localization and could be an alternative reducing substrate of *Ehi*Rr in vivo. On the other hand, *Ehi*FDP1 was detected adjacent to the cell periphery when views were taken at different depths of the cell structure (a detection pattern different to *Ehi*Rr, Fig. 8), as had been previously described [20]. Indeed, *Ehi*FDP1 and *Ehi*NROR seem to be in different sub-cellular compartments. This result supports the importance of Fds, which have already been described as cytoplasmic proteins [20,48], as potential reducing substrates for *Ehi*FDP1 in vivo.

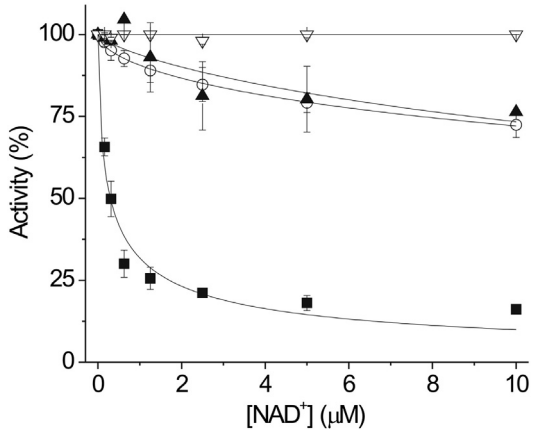

Fig. 7. Inhibition of *Ehi*NROR activity by NAD^+. NAD^+ titration curves were performed for different activities mediated by 0.1 μM *Ehi*NROR at pH 7.0 and 30 °C: NADPH oxidase (under aerobic conditions with 0.2 mM NADPH) (■), ferric-reductase activity (under microaerophilic conditions with 0.2 mM NADPH and 0.25 mM $Fe(CN)_6^{3-}$) (○), *Ehi*Rr-reduction activity (under microaerophilic conditions with 0.2 mM NADPH, 5 μM *Ehi*Rr and 25 μM H_2O_2) (▲) and Rd-reductase activity (under microaerophilic conditions with 0.2 mM NADPH and 100 μM *Cpa*Rd) (▽).

4. Discussion and conclusion

The enteric unicellular parasite *E. histolytica* is the causative agent of amoebiasis, a disease that is surpassed only by malaria and schistosomiasis for death caused by a parasitic infection [WHO, http://www.who.int/en/][51]. A critical virulence factor of the microorganism is determined by its ability to cope with conditions of increasing oxygen pressures and high ROS and RNS levels [2]. We have recently demonstrated the occurrence of TRX systems in *E. histolytica* [23,24], which functionally expands the understanding about redox metabolism in this parasite. The redox metabolic scenario operating in *E. histolytica* includes the involvement of antioxidant systems that plays a critical role in the maintenance of redox balance in the parasite. A flavodiiron protein and a rubrerythrin (two antioxidant proteins) have been characterized in this human pathogen, although their physiological reductants have not been identified [19,20,52]. In view of this, we analyzed the functionality of two redox components of different metabolic pathways to reduce *Ehi*FDP1 and *Ehi*Rr in the parasite.

Herein we performed the molecular cloning of the gene coding for a putative *Ehi*NROR, followed by its expression to produce the recombinant protein with a high purity degree. Physiologically, the NAD(P)H oxidase activity in *E. histolytica* would act as a first stage in the O_2 elimination route leading to its partial reduction to H_2O_2, thus generating ROS. It would follow neutralization of the latter compounds by reduction to H_2O toward antioxidant systems (for example, peroxidases or cysteine) to avoid cellular damages [23,24]. All the results herein presented support the fact that *Ehi*NROR is a true Rd reductase that is able to transfer electrons to Rds from bacterial origin, as well to iron-dependent ROS detoxifying enzymes such as *Ehi*Rr and *Ehi*FPD1 (with similar catalytic efficiency). The enzyme can utilize either NADPH or NADH as reducing equivalent donors for the reductase or oxidase activity, although the Rd reductase activity with NADH was higher than for NADPH. The activity exhibited by *Ehi*NROR with NADPH is noteworthy, especially if compared with NRORs exhibiting a preference toward NADH over NADPH (between two and three orders of magnitude) [43,47,53]. Surprisingly, NADPH oxidase activity of the amoebic enzyme

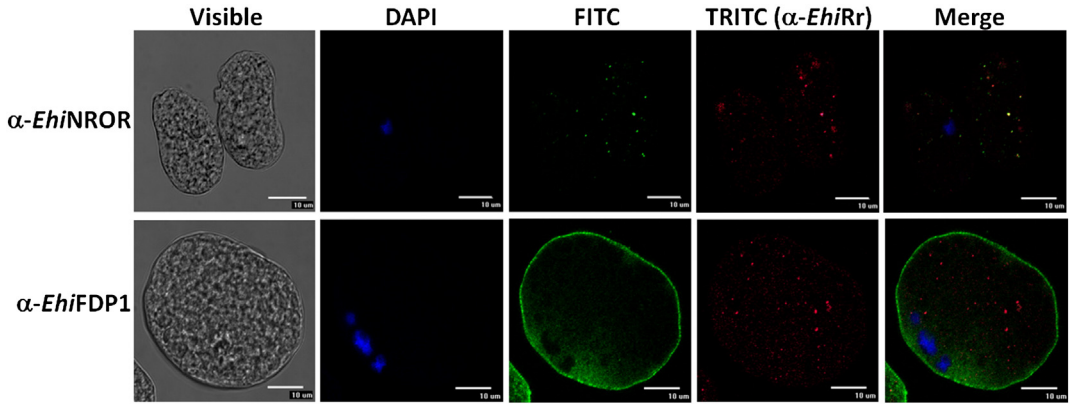

Fig. 8. Inmunodetection of *Ehi*NROR in *E. histolytica* trophozoites. Confocal microscopy images of co-inmunolocalization of *Ehi*Rr (labeled with mouse anti-*Ehi*Rr antibody and TRITC conjugated goat anti-IgG as a secondary antibody, red) and *Ehi*NROR (labeled with rabbit anti-*Ehi*NROR antibody and FITC conjugated goat anti-IgG as a secondary antibody, green) or *Ehi*FDP1 (labeled with rabbit anti-*Ehi*FDP1 antibody and FITC conjugated goat anti-IgG as a secondary antibody, green). Parasites were stained with DAPI for visualization of nucleus (blue).

presented a strong inhibition by NAD^+, with results indicating that the latter could act as a non-competitive tight-binding inhibitor. In vivo, this inhibitory behavior may act as a mechanism regulating oxidase activity and it supports a role for the enzyme other than as a direct oxygen scavenger in the parasite. Conversely, the ability to transfer electrons to other Rd-like proteins [or iron-complex, such as $Fe(CN)_6^{3-}$] was not inhibited by NAD^+. The fact that *Ehi*NROR transfers reducing equivalents to *Ehi*Rr or *Ehi*FPD1 independently of an intermediary protein is highly relevant because *E. histolytica* lacks Rds. Recently, the importance of Rd as an intermediary in such system has been questioned. For example, a *P. furiosus* mutant strain lacking Rd had unchanged its oxygen consumption capacity (via its FDP) [54]. So, it is evident that there are other proteins able to functionally replace Rd (likely Fd). Also, it was observed that NROR from *Clostridium acetobutylicum* was able to efficiently transfer electrons directly to Rr [53]. After these data it is tempting to speculate that these electronic transfer systems characteristic of anaerobic organisms do not necessarily operate in a linear step by step way, but they may act with marked plasticity with respect to reactions sequence.

Early reports showed that *E. histolytica* can present two different metabolic scenarios (anaerobic and aerobic) mainly depending on the oxygen partial tension in the environment [4,5,8]. Ethanol and CO_2 are the major endproducts of anaerobic carbohydrate metabolism. Pyruvate originated in glycolysis is converted to acetyl-CoA and CO_2 by *Ehi*PFOR, yielding electrons that are accepted by Fds. Acetyl-CoA is converted to enzyme-bound thiohemiacetal and then is further reduced to ethanol. These last two steps are catalyzed by a NAD^+-dependent bifunctional aldehyde-alcohol dehydrogenase (ADH2). Alternatively, part of the enzyme-bound thiohemiacetal hydrolyzes to free acetaldehyde, which is reduced by a distinct $NADP^+$-dependent alcohol dehydrogenase (AHD1) [4,5,8]. Under anaerobic conditions the unsolved feature is the pathway by which electrons released at the pyruvate oxidation step (reduced Fd) are transferred to NAD^+. It should be stated that in *E. histolytica* the conversion of phosphoenolpyruvate to pyruvate can course by two pathways. One involves the single reaction catalyzed by pyruvate phosphate dikinase, whereas the alternative is the sequential action of phosphoenolpyruvate carboxylase, malate dehydrogenase

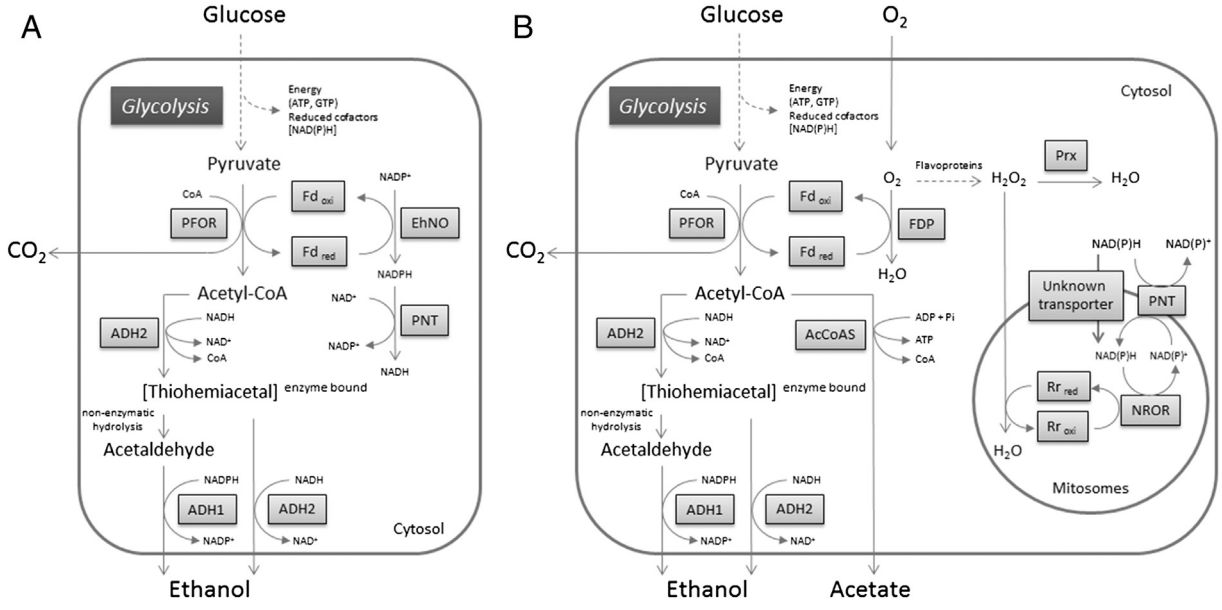

Fig. 9. Proposed in vivo reactions in the absence (A) or presence (B) of molecular oxygen. PFOR, pyruvate:ferredoxin oxidoreductase; Fd_{oxi} and Fd_{red}, oxidized and reduced form of ferredoxin; *Ehi*NO, ferredoxin:$NADP^+$ oxidoreductase; ADH1, $NADP^+$-dependent alcohol dehydrogenase; ADH2, NAD^+-dependent bifunctional aldehyde:alcohol dehydrogenase; PNT, pyridine nucleotide transhydrogenase; FDP, flavodiiron protein; AcCoAS, acetyl-CoA synthetase; Rr_{oxi} and Rr_{red}, oxidized and reduced form of rubrerythrin; NROR, rubredoxin reductase; Prx, peroxiredoxin.

and malic enzyme. The net effect of these alternative routes together with the presence of a transhydrogenase is a direct interexchange between NADH and NADPH in the parasite [5,8].

In hydrogenosome-containing organisms, under anaerobic conditions, a major means of Fd re-oxidation is via the generation of H_2. This reaction is catalyzed by hydrogenase through the transfer of electrons to protons [4,5,8]. *E. histolytica* lacks hydrogenosomes and unable to produce H_2 axenically [55]. One possible solution may be the recently characterized NADPH oxido-reductase 1 (*Ehi*NO1) [11]. This enzyme could function as an Fd:NADP reductase, being involved in the generation of NADPH and oxidized Fd [11]. Under aerobic conditions a small fraction of acetyl-CoA is converted to acetate by an acetyl-CoA synthetase. Then acetate is excreted to the extracellular medium. This indicates that part of the total reducing power generated in metabolism is transferred to O_2; however, much of reoxidation of reduced carries stills occurs via the reduction of acetyl-CoA to ethanol [4,5,8,55].

The route by which electrons from reduced equivalents are transferred to O_2 without the production of ROS in *E. histolytica* is also an unsolved matter. To date the only enzyme with the ability to reduce O_2 directly to H_2O is *Ehi*FDP1. The enzyme has a robust O_2 reductase activity, high substrate specificity and is abundantly expressed in the cytoplasm [20], thus, acting as a putative terminal oxidase. As far as we know, physiological redox partners for *Ehi*FDP1 have not been identified, the way by which this enzyme is connected to the metabolism is unknown. On the other hand, little information is available about the physiological relevance of Fds in *E. histolytica*. We are focusing our studies to gain further understanding of the importance of these proteins in this organism. We note that reduced Fds can be used by *Ehi*FDP1 (the terminal oxidase) as a physiological source of reducing equivalents. This would allow the regeneration of oxidized Fds and thus its reentry into the glycolytic pathway as oxidized cofactors.

Results in the present work allow us to propose the scenario schematized in Fig. 9, where part of the NAD(P)H produced during glycolysis could be used by *Ehi*NROR (inside mitosomes) to directly reduce *Ehi*Rr (a peroxidase protein). In this way, across both pathways the transfer of electrons from reducing equivalents to O_2 (or ROS) would be complete. To the best of our knowledge, this is the first study to characterize an NROR activity from *E. histolytica* (in fact, the first from any eukaryote), and it also establish that amoebic Fds can act as reducing donors for both *Ehi*FDP1 and *Ehi*Rr. Our results strongly support the in vivo functionality of the metabolic systems proposed in Fig. 9. It would be of great value to solve definitively the complete set of reactions that are functional in *E. histolytica* to manage redox equivalents in central metabolism or to cope with oxidative stress, because these metabolic tools are critical for the parasite maintenance and virulence.

Transparency document

The Transparency document associated with this article can be found, in the online version.

Acknowledgements

We thank Dr. Donald M. Kurtz (University of Texas at San Antonio) for providing the plasmid containing the *Thermotoga maritima* rubredoxin reductase, Dr. Michael W. W. Adams (University of Georgia) for *Pyrococcus furiosus* rubredoxin expression plasmid and Dr. Jean-Marc Moulis (Université J. Fourier) for *Clostridium pasteurianum* rubredoxin expression plasmid. We wish to thank Dr. Eduardo A. Ceccarelli (IBR — Argentina) for providing us with purified ferredoxin NADP reductase from *Pisum sativum*, ferredoxin from *P. sativum*, flavodoxin from *E. coli* and DPI-Cl. This work was supported by grants from UNL (CAI + D Orientados & Redes 2011), CONICET (PIP112-2011-0100439, PIP114-2011-0100168) and ANPCyT (PICT2012-2439). MSC is a fellow from CONICET. SAG, AAI and DGA are investigator career members from the same institution.

Appendix A. Supplementary data

Supplementary data to this article can be found online at http://dx.doi.org/10.1016/j.bbagen.2015.02.010.

References

[1] B. Loftus, I. Anderson, R. Davies, U.C. Alsmark, J. Samuelson, P. Amedeo, P. Roncaglia, M. Berriman, R.P. Hirt, B.J. Mann, T. Nozaki, B. Suh, M. Pop, M. Duchene, J. Ackers, E. Tannich, M. Leippe, M. Hofer, I. Bruchhaus, U. Willhoeft, A. Bhattacharya, T. Chillingworth, C. Churcher, Z. Hance, B. Harris, D. Harris, K. Jagels, S. Moule, K. Mungall, D. Ormond, R. Squares, S. Whitehead, M.A. Quail, E. Rabbinowitsch, H. Norbertczak, C. Price, Z. Wang, N. Guillen, C. Gilchrist, S.E. Stroup, S. Bhattacharya, A. Lohia, P.G. Foster, T. Sicheritz-Ponten, C. Weber, U. Singh, C. Mukherjee, N.M. El-Sayed, W.A. Petri Jr., C.G. Clark, T.M. Embley, B. Barrell, C.M. Fraser, N. Hall, The genome of the protist parasite *Entamoeba histolytica*, Nature 433 (2005) 865–868.
[2] M.A. Akbar, N.S. Chatterjee, P. Sen, A. Debnath, A. Pal, T. Bera, P. Das, Genes induced by a high-oxygen environment in *Entamoeba histolytica*, Mol. Biochem. Parasitol. 133 (2004) 187–196.
[3] S.D. Ladas, G. Karamanolis, E. Ben-Soussan, Colonic gas explosion during therapeutic colonoscopy with electrocautery, World J. Gastroenterol. 13 (2007) 5295–5298.
[4] M. Muller, Energy metabolism of protozoa without mitochondria, Annu. Rev. Microbiol. 42 (1988) 465–488.
[5] R.E. Reeves, Metabolism of *Entamoeba histolytica* Schaudinn, 1903, Adv. Parasitol. 23 (1984) 105–142.
[6] B. Rosenthal, Z. Mai, D. Caplivski, S. Ghosh, H. de la Vega, T. Graf, J. Samuelson, Evidence for the bacterial origin of genes encoding fermentation enzymes of the amitochondriate protozoan parasite *Entamoeba histolytica*, J. Bacteriol. 179 (1997) 3736–3745.
[7] E.C. Weinbach, L.S. Diamond, *Entamoeba histolytica*. I. Aerobic metabolism, Exp. Parasitol. 35 (1974) 232–243.
[8] J. McLaughlin, S. Aley, The biochemistry and functional morphology of the *Entamoeba*, J. Protozool. 32 (1985) 221–240.
[9] D.M. Brown, J.A. Upcroft, P. Upcroft, A H_2O-producing NADH oxidase from the protozoan parasite *Giardia duodenalis*, Eur. J. Biochem. 241 (1996) 155–161.
[10] D.G. Arias, E.L. Regner, A.A. Iglesias, S.A. Guerrero, *Entamoeba histolytica* thioredoxin reductase: molecular and functional characterization of its atypical properties, Biochim. Biophys. Acta 1820 (2012) 1859–1866.
[11] G. Jeelani, A. Husain, D. Sato, V. Ali, M. Suematsu, T. Soga, T. Nozaki, Two atypical L-cysteine-regulated NADPH-dependent oxidoreductases involved in redox maintenance, L-cystine and iron reduction, and metronidazole activation in the enteric protozoan *Entamoeba histolytica*, J. Biol. Chem. 285 (2010) 26889–26899.
[12] I.J. Anderson, B.J. Loftus, *Entamoeba histolytica*: observations on metabolism based on the genome sequence, Exp. Parasitol. 110 (2005) 173–177.
[13] E. Ramos-Martinez, A. Olivos-Garcia, E. Saavedra, M. Nequiz, E.C. Sanchez, E. Tello, M. El-Hafidi, A. Saralegui, E. Pineda, J. Delgado, I. Montfort, R. Perez-Tamayo, *Entamoeba histolytica*: oxygen resistance and virulence, Int. J. Parasitol. 39 (2009) 693–702.
[14] R.L. Krauth-Siegel, A.E. Leroux, Low-molecular-mass antioxidants in parasites, Antioxid. Redox Signal. 17 (2012) 583–607.
[15] D.P. Jones, Radical-free biology of oxidative stress, Am. J. Physiol. Cell Physiol. 295 (2008) C849–C868.
[16] M. Koharyova, M. Kolarova, Oxidative stress and thioredoxin system, Gen. Physiol. Biophys. 27 (2008) 71–84.
[17] N. Rouhier, C.S. Koh, E. Gelhaye, C. Corbier, F. Favier, C. Didierjean, J.P. Jacquot, Redox based anti-oxidant systems in plants: biochemical and structural analyses, Biochim. Biophys. Acta 1780 (2008) 1249–1260.
[18] M.R. Ariyanayagam, A.H. Fairlamb, *Entamoeba histolytica* lacks trypanothione metabolism, Mol. Biochem. Parasitol. 103 (1999) 61–69.
[19] B. Maralikova, V. Ali, K. Nakada-Tsukui, T. Nozaki, M. van der Giezen, K. Henze, J. Tovar, Bacterial-type oxygen detoxification and iron–sulfur cluster assembly in amoebal relict mitochondria, Cell. Microbiol. 12 (2010) 331–342.
[20] J.B. Vicente, V. Tran, L. Pinto, M. Teixeira, U. Singh, A detoxifying oxygen reductase in the anaerobic protozoan *Entamoeba histolytica*, Eukaryot. Cell 11 (2012) 1112–1118.
[21] I. Bruchhaus, N.W. Brattig, E. Tannich, Recombinant expression, purification and biochemical characterization of a superoxide dismutase from *Entamoeba histolytica*, Arch. Med. Res. 23 (1992) 27–29.
[22] I. Bruchhaus, E. Tannich, Induction of the iron-containing superoxide dismutase in *Entamoeba histolytica* by a superoxide anion-generating system or by iron chelation, Mol. Biochem. Parasitol. 67 (1994) 281–288.
[23] D.G. Arias, C.E. Gutierrez, A.A. Iglesias, S.A. Guerrero, Thioredoxin-linked metabolism in *Entamoeba histolytica*, Free Radic. Biol. Med. 42 (2007) 1496–1505.
[24] D.G. Arias, P.G. Carranza, H.D. Lujan, A.A. Iglesias, S.A. Guerrero, Immunolocalization and enzymatic functional characterization of the thioredoxin system in *Entamoeba histolytica*, Free Radic. Biol. Med. 45 (2008) 32–39.
[25] T.F. Maniatis, E:F, J. Sambrook, Molecular Cloning: A Laboratory Manual, Cold Spring Harbor Laboratory, Cold Spring Harbor, New York, 1982.
[26] C.G. Clark, L.S. Diamond, Methods for cultivation of luminal parasitic protists of clinical importance, Clin. Microbiol. Rev. 15 (2002) 329–341.
[27] I. Mathieu, J. Meyer, J.M. Moulis, Cloning, sequencing and expression in *Escherichia coli* of the rubredoxin gene from *Clostridium pasteurianum*, Biochem. J. 285 (Pt 1) (1992) 255–262.
[28] M.V. Weinberg, F.E. Jenney Jr., X. Cui, M.W. Adams, Rubrerythrin from the hyperthermophilic archaeon *Pyrococcus furiosus* is a rubredoxin-dependent, iron-containing peroxidase, J. Bacteriol. 186 (2004) 7888–7895.

[29] F. Hillmann, O. Riebe, R.J. Fischer, A. Mot, J.D. Caranto, D.M. Kurtz Jr., H. Bahl, Reductive dioxygen scavenging by flavo-diiron proteins of *Clostridium acetobutylicum*, FEBS Lett. 583 (2009) 241–245.
[30] M.M. Bradford, A rapid and sensitive method for the quantitation of microgram quantities of protein utilizing the principle of protein–dye binding, Anal. Biochem. 72 (1976) 248–254.
[31] U.K. Laemmli, Cleavage of structural proteins during the assembly of the head of bacteriophage T4, Nature 227 (1970) 680–685.
[32] J. Vaitukaitis, J.B. Robbins, E. Nieschlag, G.T. Ross, A method for producing specific antisera with small doses of immunogen, J. Clin. Endocrinol. Metab. 33 (1971) 988–991.
[33] M.P. Gordge, J.S. Hothersall, A.A. Noronha-Dutra, Evidence for a cyclic GMP-independent mechanism in the anti-platelet action of S-nitrosoglutathione, Br. J. Pharmacol. 124 (1998) 141–148.
[34] L. Ledesma García, E. Rivas-Marín, B. Floriano, K. Ewen, F. Reyes-Ramírez, E. Santero, ThnY is a ferredoxin reductase-like iron–sulfur flavoprotein that has evolved to function as a regulator of tetralin biodegradation gene expression, J. Biol. Chem. 286 (2011) 1709–1718.
[35] P. Eyer, F. Worek, D. Kiderlen, G. Sinko, A. Stuglin, V. Simeon-Rudolf, E. Reiner, Molar absorption coefficients for the reduced Ellman reagent: reassessment, Anal. Biochem. 312 (2003) 224–227.
[36] A.E. Chung, Pyridine nucleotide transhydrogenase from *Azotobacter vinelandii*, J. Bacteriol. 102 (1970) 438–447.
[37] A. Aliverti, B. Curti, M.A. Vanoni, Identifying and quantitating FAD and FMN in simple and in iron–sulfur-containing flavoproteins, Methods Mol. Biol. 131 (1999) 9–23.
[38] R. Chauhan, S.C. Mande, Characterization of the *Mycobacterium tuberculosis* H37Rv alkyl hydroperoxidase AhpC points to the importance of ionic interactions in oligomerization and activity, Biochem. J. 354 (2001) 209–215.
[39] C.N. Giannopolitis, S.K. Ries, Superoxide dismutases: I. Occurrence in higher plants, Plant Physiol. 59 (1977) 309–314.
[40] M.N. Nagi, A.M. al-Bekairi, H.A. al-Sawaf, Spectrophotometric assay for superoxide dismutase based on the nitroblue tetrazolium reduction by glucose–glucose oxidase, Biochem. Mol. Biol. Int. 36 (1995) 633–638.
[41] G. Hagelueken, L. Wiehlmann, T.M. Adams, H. Kolmar, D.W. Heinz, B. Tummler, W.D. Schubert, Crystal structure of the electron transfer complex rubredoxin rubredoxin reductase of *Pseudomonas aeruginosa*, Proc. Natl. Acad. Sci. U. S. A. 104 (2007) 12276–12281.
[42] D.M. Kurtz Jr., Avoiding high-valent iron intermediates: superoxide reductase and rubrerythrin, J. Inorg. Biochem. 100 (2006) 679–693.
[43] K. Ma, M.W. Adams, NAD(P)H:rubredoxin oxidoreductase from *Pyrococcus furiosus*, Methods Enzymol. 334 (2001) 55–62.
[44] P. Macheroux, UV–visible spectroscopy as a tool to study flavoproteins, Methods Mol. Biol. 131 (1999) 1–7.
[45] Z. Cheng, L.D. Arscott, D.P. Ballou, C.H. Williams Jr., The relationship of the redox potentials of thioredoxin and thioredoxin reductase from *Drosophila melanogaster* to the enzymatic mechanism: reduced thioredoxin is the reductant of glutathione in *Drosophila*, Biochemistry 46 (2007) 7875–7885.
[46] S. Chakraborty, V. Massey, Reaction of reduced flavins and flavoproteins with diphenyliodonium chloride, J. Biol. Chem. 277 (2002) 41507–41516.
[47] K. Ma, M.W. Adams, A hyperactive NAD(P)H:rubredoxin oxidoreductase from the hyperthermophilic archaeon *Pyrococcus furiosus*, J. Bacteriol. 181 (1999) 5530–5533.
[48] M.A. Rodriguez, R.M. Garcia-Perez, L. Mendoza, T. Sanchez, N. Guillen, E. Orozco, The pyruvate:ferredoxin oxidoreductase enzyme is located in the plasma membrane and in a cytoplasmic structure in *Entamoeba*, Microb. Pathog. 25 (1998) 1–10.
[49] R.E. Reeves, J.D. Guthrie, P. Lobelle-Rich, *Entamoeba histolytica*: isolation of ferredoxin, Exp. Parasitol. 49 (1980) 83–88.
[50] Y. Lehmann, L. Meile, M. Teuber, Rubrerythrin from *Clostridium perfringens*: cloning of the gene, purification of the protein, and characterization of its superoxide dismutase function, J. Bacteriol. 178 (1996) 7152–7158.
[51] J.A. Walsh, Problems in recognition and diagnosis of amebiasis: estimation of the global magnitude of morbidity and mortality, Rev. Infect. Dis. 8 (1986) 228–238.
[52] V.L. Goncalves, J.B. Vicente, L. Pinto, C.V. Romao, C. Frazao, P. Sarti, A. Giuffre, M. Teixeira, Flavodiiron oxygen reductase from Entamoeba histolytica: modulation of substrate preference by tyrosine 271 and lysine 53, J. Biol. Chem. 289 (2014) 28260–28270.
[53] O. Riebe, R.J. Fischer, D.A. Wampler, D.M. Kurtz Jr., H. Bahl, Pathway for H_2O_2 and O_2 detoxification in *Clostridium acetobutylicum*, Microbiology 155 (2009) 16–24.
[54] M.P. Thorgersen, K. Stirrett, R.A. Scott, M.W. Adams, Mechanism of oxygen detoxification by the surprisingly oxygen-tolerant hyperthermophilic archaeon, *Pyrococcus furiosus*, Proc. Natl. Acad. Sci. U. S. A. 109 (2012) 18547–18552.
[55] R.E. Reeves, L.G. Warren, B. Susskind, H.S. Lo, An energy-conserving pyruvate-to-acetate pathway in *Entamoeba histolytica*. Pyruvate synthase and a new acetate thiokinase, J. Biol. Chem. 252 (1977) 726–731.